JACS
JOURNAL OF THE AMERICAN CHEMICAL SOCIETY
pubs.acs.org/JACS
Article

Direct Conversion of N_2 and Air to Nitric Acid in Gas–Water Microbubbles

Sandeep Bose, Mohammad Mofidfar, and Richard N. Zare*

Cite This: https://doi.org/10.1021/jacs.4c11899
Read Online
ACCESS | Metrics & More | Article Recommendations | Supporting Information

ABSTRACT: We report a simple, direct, and green conversion of air/N_2 to nitric acid by bubbling the gas through an aqueous solution containing 50 μM Fe^{2+} ions. Air stone, along with ultrasonication, was employed to generate gas microbubbles. H_2O_2 produced at the water–gas interface undergoes Fenton's reaction with Fe^{2+} ions to produce $OH^{\bullet}$ that efficiently activates N_2, yielding nitric acid as the final product. Nitrate (NO_3^-) formation occurs without the use of any external electric potential or radiation. The concentration of NO_3^- increased linearly with time over a period of 132 h. The average NO_3^- production rate is found to be 12.9 ± 0.05 μM h^{-1}. We envision that this nitrogen fixation strategy that produces nitric acid in an eco-friendly way might open the possibility for the energy-efficient and green production of nitric acid.

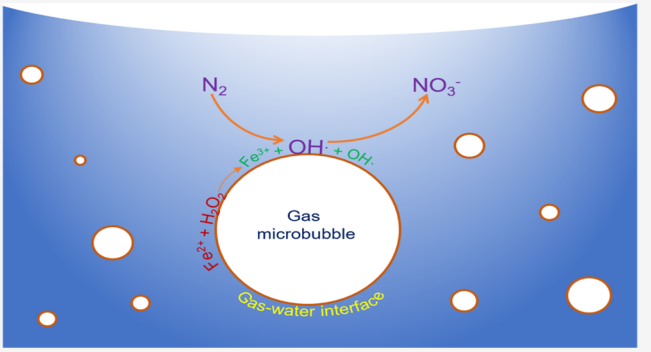

INTRODUCTION

The global market for nitric acid production reached approximately 57 million tons in 2023 and is expected to increase to 70 million tons by 2032, most of which is and will continue to be used in the production of fertilizers.[1] Thus, HNO_3 should be considered a large commodity chemical. Nearly all of the HNO_3 produced in the U.S. is manufactured by the high-temperature catalytic oxidation of ammonia (NH_3).[2] This is accomplished in a three-step process. First, a 1:9 ammonia/air mixture is oxidized at a temperature of 1380–1470 °F as it passes through a catalytic converter, according to the following reaction: $4NH_3 + 5O_2 \rightarrow 4NO + 6H_2O$. The most common catalyst is made of 90% platinum and 10% rhodium gauze constructed from squares of fine wire. In the second step, the process stream is passed through a condenser and cooled to 100 °F or less at pressures up to 116 pounds per square inch. The nitric oxide (NO) reacts with residual oxygen (O_2) to form nitrogen dioxide (NO_2) and its liquid dimer, nitrogen tetroxide (N_2O_4). The reaction is $4NO + 2O_2 \rightarrow 2NO_2 + N_2O_4$. The third and final step is to add this liquified stream to deionized water. The exothermic reaction ensued as $3NO_2 + H_2O \rightarrow 2HNO_3 + NO$. A secondary airstream is introduced to oxidize the NO. The resulting HNO_3 concentration varies from 30% to 70% depending upon the temperature, pressure, number of water reaction stages, and concentration of the nitrogen oxides initially entering the final stage.

As can be appreciated, the above process is highly energy-intensive. It particularly suffers from the use of ammonia, which is generated by the Haber–Bosch process, a process that is also highly energy-intensive and releases carbon dioxide from the steam reforming conversion of methane (CH_4) into hydrogen (H_2) for combining with nitrogen (N_2).[2] Consequently, it would be highly desirable to find an eco-friendly means of making HNO_3. Recently, Banerjee and co-workers[3] have found that air nitrogen reacts with water droplets at the air–water interface, fixing molecular nitrogen to its oxides (NO, NO_2, and N_2O) and acids (HNO_2 and HNO_3) at trace levels at room temperature without any catalyst. They also showed that bubbling N_2 through water with an average bubble size of 2 mm yielded nitrite (NO_2^-) and nitrate (NO_3^-) anions at trace levels, as detected mass spectrometrically. Independently, we have also investigated the formation of nitrate anions by passing micron-sized N_2 bubbles through water with the addition of a Fe^{2+}. We have shown that nitric acid can be easily produced by this means at room temperature and atmospheric pressure without any use of an external electric field or radiation. If this process could be economically scaled, we suggest that it would represent a major advance in making a more sustainable world. Our work differs from the previous study by Banerjee and co-workers in that we use microbubbles, the use of ferrous ions in solution to promote

Received: August 28, 2024
Revised: September 14, 2024
Accepted: September 16, 2024

the formation of the hydroxyl radical ($OH^{\bullet}$) from the decomposition of hydrogen peroxide (H_2O_2), all of which greatly enhances nitrate formation.

Water is regarded as a stable and relatively inert molecule in bulk solution. However, water behaves exceptionally near the water−air interface of micrometer-sized gas bubbles or water microdroplets, giving rise to redox reactions and a cascade of radical-initiated chemical transformations. At the interface, water is spontaneously oxidized to form hydrogen peroxide (H_2O_2).[4,5] This process does not require any chemical reagent, catalyst, applied electric potential, or radiation. The air−water interface of a microbubble or a microdroplet has a strong electric field, on the order of 10^9 V m^{-1}.[6,7] At the interface, the hydronium ions and hydroxide ions are separated and heterogeneously distributed, which enhances the electric field strength.[8] At the air−water surface, it is also not possible to have three-dimensional solvation of the H^+ and OH^- ions, which further promotes radical formation.[9] This electric field strength is sufficient to ionize hydroxide ions to form hydroxyl radicals, which recombine into H_2O_2. The exceptional electric field at the air−water interface was previously shown to accelerate reaction rates and lead to the formation of unexpected products.[10−25] Electric field-driven redox reactions at the gas−liquid interface of the microdroplets were previously studied.[26−28] Recently, Ciampi et al. have shown that electrochemical reactions can also take place at the interface of a microbubble,[14] which led us to believe that microdroplets and microbubbles show similar chemistry at the interface. Here, we demonstrated that the H_2O_2 produced at the gas−water interface plays a crucial role in our microbubble-based HNO_3 production by initiating Fenton's reaction at the gas microbubble interface:[29−32]

$$Fe^{2+} + H_2O_2 \rightarrow Fe^{3+} + OH^{\bullet} + OH^- \quad (1)$$

METHOD

A reaction system (Figure 1) is designed that mainly consists of three components: an ultrasonic bath, a temperature controller, and a continuous gas flow. A beaker with 20 mL of water containing 50 μM $FeSO_4$ is placed in an ultrasonic bath. Air/N_2 is slowly bubbled into the solution at 50 psi through a cylindrical porous mineral bubbler called an air stone to produce microbubbles. Air/N_2 serves as a nitrogen source for the HNO_3 formation. We employed an activated carbon filter to remove any HNO_3 impurities in the gas flow.

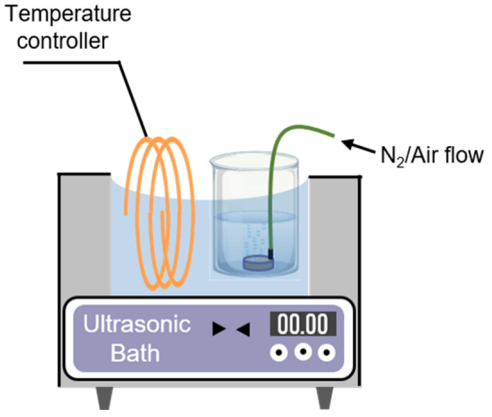

Figure 1. Schematic of the experimental setup for HNO_3 production.

Ultrasonication is employed while bubbling to further produce fine microbubbles. A temperature controller is introduced to counteract any increase in the temperature of the bath caused by its continuous operation. In addition, a stable temperature does not allow the reaction products to degrade or evaporate during the reaction. Even so, some evaporation occurs over time, and we add water every 2 h to maintain the same amount of water. Continuous bubbling is carried out under sonication for 6 h, and then the products are analyzed.

RESULTS AND DISCUSSION

The formation of H_2O_2 in the droplets was confirmed by peroxide testing strip assays and quantified using the potassium titanium oxalate (PTO)-based spectrophotometric (colorimetric) method by measuring the absorbance at 400 nm. Figure S1 visually demonstrates the presence of H_2O_2 in the microbubbled sample at different bubbling times. Figure 2A presents the plot of the H_2O_2 concentration obtained due to Fe^{2+} upon continuous bubbling of N_2 over an extended period. The whole experiment for H_2O_2 was replicated three times, and the average values of three different measurements were reported and plotted in the graph. The uncertainties were reported in terms of error bars. After 6 h, the H_2O_2 concentration measured was 0.5 mM, which increases linearly with time up to 72 h. During this period, the rate of production of H_2O_2 was estimated to be 72.6 ± 3.6 μM h^{-1}. At 72 h, the H_2O_2 concentration was found to be 5.4 mM. We performed a control experiment to check the H_2O_2 formation in the absence of Fe^{2+}. We observed a very low quantity of H_2O_2 in the absence of Fe^{2+}, whereas Fe^{2+} substantially enhances the H_2O_2 production (Figure S2). This indicates that the presence of Fe^{2+} not only initiates Fenton's reaction but also plays a role in enhancing the H_2O_2 production. Thus, the concentration of H_2O_2 produced due to Fe^{2+} only is obtained by subtracting the H_2O_2 concentration of the solution in the absence of Fe^{2+} from the H_2O_2 concentration of the solution in the presence of Fe^{2+}, which is plotted against time in Figure 2A.

Although H_2O_2 tends to evaporate or degrade at ambient conditions, we observed a steady increase in the H_2O_2 production caused by the continuous generation of microbubbles in the solution. Besides, the employment of ultrasonication further produces fine bubbles. Smaller bubble sizes are known to produce higher concentrations of H_2O_2. Nonetheless, some evaporation occurs over time, and we added water to the marked container every 2 h to maintain the same water level. All of these combined factors resulted in an increase in H_2O_2 concentration in the solution. This also helped us not to concentrate NO_3^- over time, so that we obtained a fairly accurate concentration of NO_3^-.

Fenton's reaction produces $OH^{\bullet}$, which is vital for the oxidation of N_2 to nitrate, as previously demonstrated by electrochemistry.[33] To prove the existence of $OH^{\bullet}$ in the microdroplets, we performed a mass spectrometry analysis of the sample in the positive ion mode. The mass spectrum (Figure 2B) of the sample displays a peak at m/z 36 arising from the hydroxyl radical adduct with a hydronium cation $[OH^{\bullet} + H_3O]^+$, which has been previously identified.[34] The presence of a peak at m/z 36 confirms the generation of $OH^{\bullet}$ in the microdroplets. Additional peaks at m/z 37 and 41 are likely from $[H_2O + H_3O]^+$ and $[H_2O + Na]^+$, respectively. A possible interference at m/z 36 could be due to $[NH_4OH + H]^+$, which arises if NH_3 is formed as a product. However, when we tested the reaction product spectrophotometrically

https://doi.org/10.1021/jacs.4c11899
J. Am. Chem. Soc. XXXX, XXX, XXX−XXX

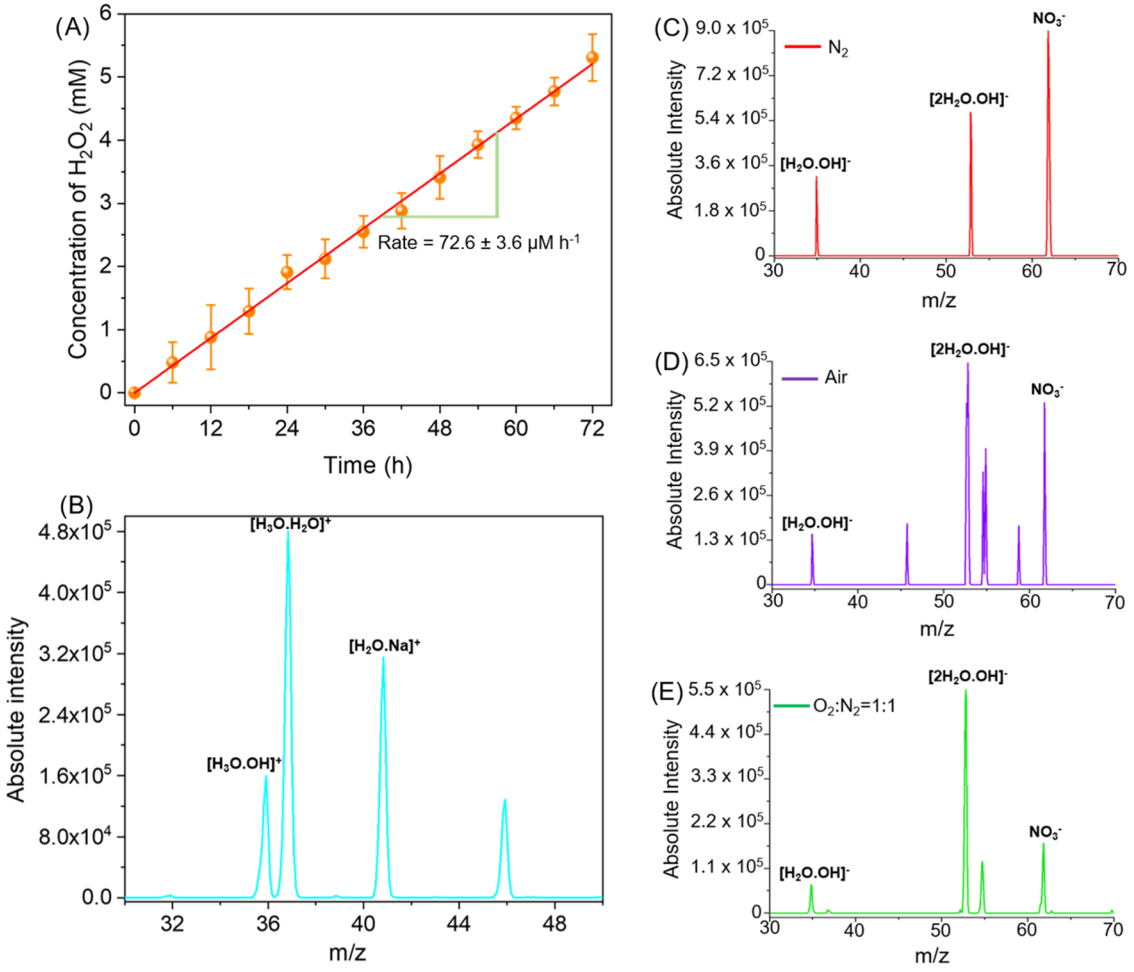

Figure 2. (A) Production of H_2O_2 as a function of time upon continuous bubbling of N_2 into the solution. (B) Mass spectrum of OH radicals generated as a result of Fenton's reaction in the microdroplets. (C–E) Mass spectra of the reaction product obtained after bubbling with compressed N_2, air, and a 1:1 mixture of N_2 and O_2 for 12 h, respectively. The mass spectra are recorded in negative ion mode.

for NH_3, as shown by Li et al.,[35] as well as with a commercially available NH_3 testing kit, we did not observe any NH_3 formation. Hence, we conclude that the peak at m/z 36 corresponds to $OH^•$.

Water microdroplets are known to produce $OH^•$. So, we performed a control study without using Fe^{2+}. It also shows the existence of $OH^•$ in the mass spectrum. However, the absolute intensity of $OH^•$ (up to the order of 10^3) produced is very low compared to the absolute intensity of $OH^•$ (up to the order of 10^5) when Fe^{2+} is used in the system. Since I_{OH} without Fe^{2+} $\ll$ I_{OH} with Fe^{2+}, I_{OH} of overall solution is almost the same with I_{OH} with Fe^{2+}. Thus, we can conclude that the concentration of $OH^•$ produced without Fe^{2+} is negligible in comparison to the $OH^•$ produced in the presence of Fe^{2+}, and the mass spectrum shown in Figure 2B almost completely corresponds to the $OH^•$ generated by Fe^{2+}.

The detection of H_2O_2 and $OH^•$ in the presence of aqueous Fe^{2+} solution confirms that Fenton's reaction occurs at the gas–water interface. The activation energy for the Fenton reaction was previously found to be 31.5 kJ mol^{-1}.[36] The low value suggested that the oxidation reaction progressed with a low energy barrier. The electric field at the air–water interface of the microdroplets is up to the order of 10^9 V m^{-1}. We believe this high electric field at the interface is sufficient to provide the activation energy necessary to overcome the energy barrier. A comparative study was done to check the efficient formation of NO_3^- from N_2, air, and an N_2:O_2 (~1:1) mixture. Each of the gases (N_2, air)/gas mixture (N_2:O_2 ~1:1) was individually bubbled into the aqueous Fe^{2+} solution for 12 h. The reaction products formed during the process were analyzed by using a linear ion trap (LTQ) mass spectrometer. We observed that when the compressed N_2 was used as a source, the highest concentration of NO_3^- was formed (Figure 2C). The mass spectrum analysis of the products operated in negative mode shows a feature at m/z 62 corresponding to the NO_3^- peak. Several other features include m/z at 35 and 53 from the $[OH + H_2O]^-$ and $[OH + 2H_2O]^-$, respectively, indicative of the hydroxide anion that results from the production of $OH^•$ produced during Fenton's reaction. The intensity ratio, I_{62}/I_{53} ~1.61, conveys the effectiveness of the conversion to NO_3^-. The introduction of compressed air (N_2:O_2 ~4:1) as the feed gas slightly diminished (I_{62}/I_{53} ~0.8) the NO_3^- production (Figure 2D). We also varied the feed gas proportion (N_2:O_2 ~1:1) to understand the role of N_2 and O_2 in the formation of NO_3^-. We notice a gradual decrease in the formation of NO_3^- (I_{62}/I_{53} ~0.4) with an increase in the oxygen content of the feed gas (Figure 2E). Because the formation of NO_3^- involves oxygen, H_2O serves as the oxygen provider for the conversion. Surprisingly, in our experiment, we have not observed any nitrite (NO_2^-) formation, as previously

https://doi.org/10.1021/jacs.4c11899
J. Am. Chem. Soc. XXXX, XXX, XXX–XXX

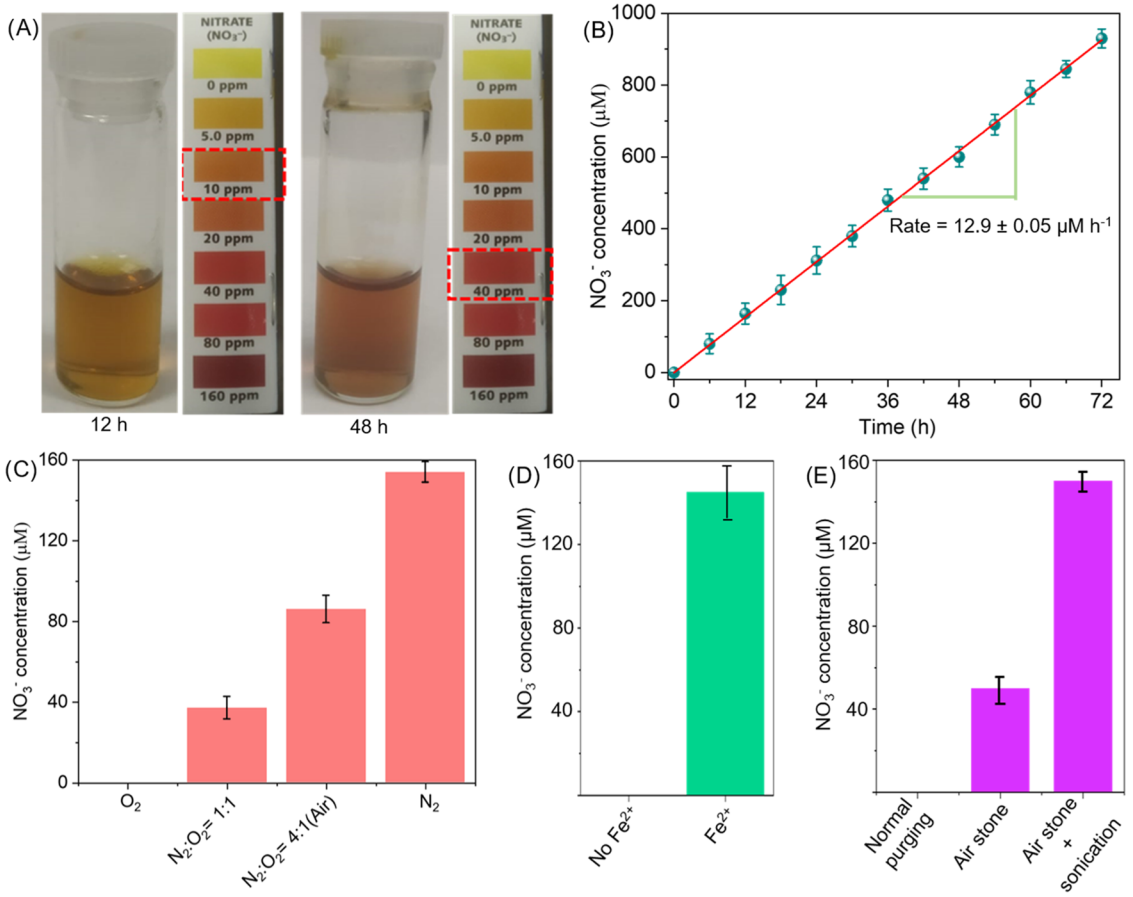

Figure 3. (A) Photographic image of the N_2-bubbled solution after 12 and 48 h upon treatment with the NO_3^- test kit. (B) Yield of NO_3^- as a function of the N_2 bubbling time. The rate of NO_3^- was found to be 12.7 μM h^{-1}. (C) Production of NO_3^- at different N_2/O_2 pressure ratios. (D) Comparison of NO_3^- yield in the presence and absence of Fe^{2+} ions. (E) Comparison of the NO_3^- concentration in the solution when different bubbling methods were employed. The whole experiment for NO_3^- was replicated three times, and the average values of three different measurements were reported and plotted in the graph. The uncertainties were reported in terms of error bars.

reported by Banerjee and co-workers.[3] We obtained nitrate as the final product and the only product, possibly because nitrate is thermodynamically more stable. The $OH^\bullet$ produced by Fenton's reaction reacts rapidly to produce nitrate as the final product. As shown in our proposed mechanism, NO_2^- could be produced as an intermediate, but in the presence of $OH^\bullet$, it is rapidly converted to nitrate.

The NO_3^- peak originates from the production of HNO_3 in the microbubbles. The formation of HNO_3 is confirmed by a change in pH after the reaction. Initially, the pH of the aqueous Fe^{2+} solution is ~6, which changes to pH ~ 4 after bubbling N_2 for 72 h (Figure S3A). Besides, the UV−vis absorption spectrum of the reaction product shows a peak at 304 nm, which matches well with the control HNO_3 (Figure S3B). These experiments confirmed the existence of HNO_3 in the solution.

To further strengthen our mass spectral interpretation, we performed colorimetric detection of the NO_3^-. We tested the sample using a nitrate test kit (API, Mars Fishcare, Chalfont, PA) that provides both qualitative and quantitative information. The kit contains NO_3^- test solution, which is added to the sample in the required amount, shaken, and kept for 5 min to observe any color change in the sample solution. Depending on the color observed, the concentration of NO_3^- in the solution was estimated. When the yellow NO_3^- test solution was added to the control, no change in color was noticed, as expected. Interestingly, upon the addition of NO_3^- test solution after 12 h air bubbling, the sample showed a minute change in color from light yellow to dark yellow, indicating a small amount of NO_3^- formation during the bubbling. As per the test chart, we believe roughly 5 ppm (~80 μM) of NO_3^- is formed. The image of the air-bubbled sample adjacent to the test chart is shown in Figure S4. To our delight, we observed a significant color change when the N_2-bubbled sample was tested with a NO_3^- test solution, and the color changes from light yellow to brownish, suggesting roughly 10 ppm (~161 μM) of NO_3^- formation.

As most of our bubbling experiments were conducted for 12 h, we checked whether an increase in bubbling time of more than 12 h has any influence on the productivity of NO_3^-. We noticed when the N_2 was bubbled for 48 h and tested with a NO_3^- test kit, the color changed to dark brown, indicating the formation of 40 ppm (~645 μM) of NO_3^- (Figure 3A).

Although the NO_3^- test kit provides qualitative and quantitative information about NO_3^- by simple visualization, the estimation only gives a rough value and is unable to convey the exact concentration. For example, when the NO_3^- concentration is ~3 ppm (48 μM), it is difficult to determine this value from the NO_3^- test chart because the color change will be very minute, and the naked eye cannot distinguish that color (both 0 and 5 ppm show yellow color in the test chart). Therefore, we externally prepared the NO_3^- testing solution

https://doi.org/10.1021/jacs.4c11899
J. Am. Chem. Soc. XXXX, XXX, XXX−XXX

using sulfanilamide, hydrochloric acid (HCl), and *N*-1-(naphthyl)-ethylenediamine dihydrochloride (NEDA).[37] The NO_3^- concentration was determined spectrophotometrically instead of by visual identification, which gives an accurate determination of NO_3^- concentration. The details of the process are discussed in the Supporting Information.

We have inserted an activated carbon filter in the gas flow to remove HNO_3 vapors, if any, present in the air. However, when the experiment was performed without the filter, we did not observe a significant change in the final yield of HNO_3 (Figure S5). This suggests air/N_2 contains very little HNO_3 and does not affect our results. Figure 3B presents a plot of time-dependent NO_3^- production upon bubbling N_2 into the aqueous Fe^{2+} solution. We observed a linear increase in the NO_3^- concentration over time on continuous bubbling. After 6 h, the NO_3^- concentration was 80 μM, which rose to 930 μM after 72 h. The substantial enhancement in the concentration just by simple bubbling for longer hours suggests that our technique may have the potential to serve as a selective method for large-scale industrial production of HNO_3. The NO_3^- production rate was calculated to be 12.9 ± 0.05 μM h^{-1}, which is significantly lower than the H_2O_2 production rate of 72.6 ± 3.6 μM h^{-1}. This suggests a small quantity of the total H_2O_2 produced is involved in the NO_3^- formation and the rest of the H_2O_2 was either decomposed, involved in other reactions, or left unreacted in the solution. When the reaction products were analyzed after 12 h, we detected 57 μM of H_2O_2, along with NO_3^-, which shows the presence of unreacted H_2O_2 in the solution even after NO_3^- formation (Figure S6). We also started the N_2-bubbling experiment with some known concentration of HNO_3 (40 μM) to check whether we observe an increase in the NO_3^- concentration or not after 12 h. To our delight, we observed an increase in the NO_3^- concentration (Figure S7), indicating the presence of NO_3^- in the solution before starting the experiment does not affect the reaction in microbubbles. We also note that the bubbles generated do not burst inside the solution.

After 72 h, the NO_3^- production rate decreases to 7.8 ± 0.25 μM h^{-1} (Figure S8). The reduction in the NO_3^- formation rate after 72 h can be directly correlated to the H_2O_2 production rate. When measured after 72 h, the H_2O_2 production significantly reduces to 59.1 ± 1.1 μM h^{-1} (Figure S9). Although a temperature controller was employed along with the sonication, we observed a slow increase in temperature when the experiment was conducted for a longer time (Figure S10). The initial temperature of the solution before the start of the experiment was 20 °C, which reached 31 °C after 72 h of sonication. After 72 h, the temperature showed a significant enhancement and reached 55 °C after 132 h. A substantial increase in the rate of temperature causes the decomposition of H_2O_2 produced during the reaction. Because the formation of H_2O_2 ($OH^\bullet$ via Fenton's reaction) is essential for the activation of N_2 to NO_3^-, a diminution in the rate of H_2O_2 production is reflected in the NO_3^- production. Nevertheless, we achieved a concentration of 1.39 mM NO_3^- after 132 h (see Figure S8).

Additional confirmation of the NO_3^- includes a ^{15}N-isotope experiment and X-ray photoelectron spectroscopy (XPS) of the reaction product. When $^{14}N_2$ was employed, the final product showed a distinct $^{14}NO_3^-$ (m/z = 62) feature. However, upon employment of $^{15}N_2$, a peak owing to $^{15}NO_3^-$ appears (m/z = 63) (Figure S11A). These observations provide concrete evidence that the generation of NO_3^- was caused by the oxidation of N_2 occurring in the microbubbles. N 1s XPS spectrum of the reaction product shows a feature at 408.3 eV, which also confirms the presence of NO_3^- in the sample (Figure S11B).[38]

Figure 3C presents a comparative study on the nitrate yield when O_2, N_2, air, and O_2:N_2 (∼1:1) were used as feed gas for 12 h. Blank testing was initially conducted using pure O_2 as the feed gas. No NO_3^- was detected when O_2 was introduced for bubbling, indicating that the reaction system was not contaminated with nitrogen species that could result in the formation of NO_3^-. Although the sample solution contains a tiny amount of dissolved air that may produce NO_3^-, we have not observed any detectable amount of NO_3^-. When N_2 was introduced into the system along with O_2 (N_2:O_2 ∼ 1:1) and continuously bubbled for 12 h, we detected a considerable amount of NO_3^- (∼37 μM) in the system. Compressed air (PN_2:PO_2 ∼4:1) as feed gas further increases the productivity (∼86 μM). The highest NO_3^- productivity was achieved when pure N_2 was employed as a feed gas for bubbling (∼154 μM). Even though compressed air is not the best condition for achieving the highest NO_3^- productivity, it shows the feasibility of directly using air for synthesizing NO_3^-. From the NO_3^- yield data, we find that increasing the O_2 content in the feed gas decreases the NO_3^- production. The dissolved O_2 may cause the formation of perhydroxyl radicals that interfere with the NO_3^- formation.

The introduction of Fe^{2+} ($FeSO_4$) into the system is essential for the formation of NO_3^-. No NO_3^- was formed in the absence of Fe^{2+} (Figure 3D), whereas a substantial amount of NO_3^- was produced (∼145 μM) when Fe^{2+} was added to the system. Banerjee and co-workers have previously shown the conversion of nitrogen to nitric acids upon nitrogen bubbling without using Fe^{2+}.[3] In our case, it is possible that some HNO_3 has formed in the absence of Fe^{2+}, but the concentration is too small to be detected by the nitrate testing solution. The detection limit of the nitrate test kit is in the range 0.02−2 μM (Griess-Ilosvay method). Even if some HNO_3 was formed in the absence of Fe^{2+}, the concentration may be below the detection limit of the nitrate test kit. Hence, we do not see any HNO_3 in the absence of Fe^{2+}.

We also quantified the NO_3^- formed during bubbling by mass spectrometry. The experimental details of the quantification are described in the Supporting Information. Figure S12A shows the mass spectrum of the standard solutions (along with the internal standard), and Figure S12B presents the corresponding calibration curve. The mass spectrometric data of the microbubbled solutions (along with the internal standard) at different time intervals are shown in Figure S13. From the mass spectrometric quantification, the yields of NO_3^- estimated are 138 μM, 298 μM, 460 μM, 595 μM, 770 μM, and 905 μM after 12, 24, 36, 48, 60, and 72 h of bubbling, respectively. We also compared the concentration values obtained by using mass spectrometry and colorimetry when the sample was bubbled for 12 h, and we see that there is not much difference in the concentration of the NO_3^- obtained using both these methods (Figure S14). Thus, we can conclude that both methods are equally competitive and accurate in determining the concentration of nitrate.

When N_2 was simply purged into the aqueous Fe^{2+} solution, no detectable amount of NO_3^- was found (Figure 3E). In contrast, when microbubbles were produced by passing N_2 through the air stone (microbubble size <500 μm), we observed a considerable quantity of NO_3^- in the system (∼48

https://doi.org/10.1021/jacs.4c11899
J. Am. Chem. Soc. XXXX, XXX, XXX−XXX

μM). However, the highest productivity was accomplished by combining air stone and sonication (~148 μM). The employment of sonication produces fine microbubbles, which results in more $OH^{\bullet}$ and more H_2O_2 production, which ultimately enhances the NO_3^- yield. These experiments show the necessity of microbubbles and their interfacial chemistry for NO_3^- production.

To understand whether the interface of microbubble and microdroplet shows similar properties, we conducted our experiment in microdroplets and measured the mass spectrum after online spray. The mass spectrum (Figure S15) also shows a peak at m/z 62 corresponding to NO_3^-. This experiment suggests that, in our case, both the microdroplet and microbubbles showed similar redox properties at the interface, which led to the formation of NO_3^-.

The effect of the concentration of $FeSO_4$ on the productivity of NO_3^- was also investigated. We found that the yield of NO_3^- rises initially and then decreases with the increase in the $FeSO_4$ concentration (Figure S16). Since microbubble reactions occur at the interface, an increase in the concentration of $FeSO_4$ increases the number of Fe^{2+} ions at the interface and promotes Fenton's reaction and N_2 activation to yield NO_3^-. Once the interface is saturated, a further increase in concentration pushes the excess Fe^{2+} to the bulk solution, where they are not involved in H_2O_2 generation or N_2 activation. Instead, the excessive Fe^{2+} reacts with $OH^{\bullet}$ via the following reaction:[33]

$$OH^{\bullet} + Fe^{2+} \rightarrow OH^- + Fe^{3+} \quad (2)$$

As a result, introducing too much Fe^{2+} decreases the $OH^{\bullet}$ concentration. This negatively impacts the activation of N_2, which is reflected in the final yield of NO_3^-.

In the microbubble conversion of air/N_2 to NO_3^-, Fe^{2+} acts as a catalyst. The Fe^{3+} generated during the process was electrochemically reduced to Fe^{2+} at the interface via the following reaction:

$$Fe^{3+} + H_2O_2 \rightarrow Fe^{2+} + HO_2^{\bullet} + H^+ \quad (3)$$

The H_2O_2 produced during the reaction process reacts with Fe^{3+} to regenerate Fe^{2+} along with perhydroxyl radical in the system.[33] Since a fraction of H_2O_2 is used to regenerate Fe^{2+} by reacting with Fe^{3+}, a small quantity of total H_2O_2 is utilized to produce NO_3^-. This explains the lower rate of production of NO_3^- (12.9 ± 0.05 μM h^{-1}) compared to that of H_2O_2 (72.6 ± 3.6 μM h^{-1}). XPS data further support the catalytic regeneration of Fe^{2+}. When XPS of aqueous Fe^{2+} solution was measured before the reaction, Fe $2p_{3/2}$ showed a peak at 709.2 eV that corresponded to Fe^{2+} (Figure S17A).[39] After 72 h of reaction in the aqueous system, no shift in the peak position or emergence of a new peak toward higher binding energy (711.7 eV for Fe^{3+}) was observed (Figure S17B).[39] Additionally, the Fe 3p display feature at 53.7 eV for Fe^{2+} before the reaction (Figure S17C) matches well with the Fe 3p feature (53.7 eV) after the reaction (Figure S17D).[39] These observations confirm the catalytic regeneration of Fe^{2+}. If the reaction had followed a nonelectrochemical pathway, the Fe^{3+} generated would have formed a $Fe(OH)_3$ precipitate, which is detrimental to the regeneration of Fe^{2+}.To our delight, we have not observed Fe^{3+} features from our XPS measurements. This suggests that the electric field-driven electrochemical pathway at the gas–liquid interface of the microbubbles is responsible for the regeneration of Fe^{2+} in the system.

To confirm the regeneration of Fe^{2+} involves perhydroxyl radical production, as mentioned in eq 3, we employed TEMPO, a spin trap, to capture the reactive oxygen species (ROS) in the system.[40] The TEMPO was spiked into the water to capture critical ROS during the microdroplet reaction. Figure 4 presents the mass spectrum of the TEMPO-captured

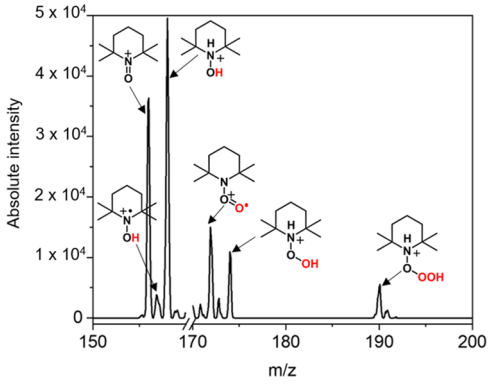

Figure 4. Mass spectrum of the radicals and reactive intermediates captured by TEMPO during N_2 oxidation.

ROS. The existence of the $H^{\bullet}$ radical was confirmed by the ion at m/z 157 (TEMPO-H) and m/z 158 (TEMPO-H-H). A peak at m/z 174 (TEMPO-H-OH) proved the existence of $OH^{\bullet}$ generated from Fenton's reaction. Interestingly, we observed a fairly strong intensity peak at m/z 190 that corresponds to TEMPO-H-OOH. From the TEMPO spin-trap experiment, it can be concluded that $HO_2^{\bullet}$ is produced during the reaction and it could be from the reduction of Fe^{3+} in the presence of H_2O_2 to regenerate Fe^{2+} in the system for further catalytic activity. Besides, droplets at the interface are rich in electrons, which possibly reduce the Fe^{3+} to Fe^{2+}. Fe^{2+} regeneration might also occur via the following pathway:

$$Fe^{3+} + OH^- \rightarrow Fe^{2+} + OH^{\bullet} \quad (4)$$

Based on our investigation, we propose a reaction pathway for the microbubble conversion of air/N_2 to NO_3^-: (1) spontaneous production of H_2O_2 at the gas–water interface; (2) the in situ-generated H_2O_2 undergoing Fenton's reaction in the presence of Fe^{2+} to produce $OH^{\bullet}$; (3) activation of N_2 by $OH^{\bullet}$ to give NO_3^-; and (4) regeneration of Fe^{2+} from Fe^{3+} by reacting with H_2O_2. We believe the conversion of N_2 to NO_3^- by $OH^{\bullet}$ activation goes through a series of sequential transformations, as suggested by Chen et al.[33] This involves the following steps:

$$N_2 \xrightarrow{OH^{\bullet}} H_2N_2O_2 \xrightarrow{OH^{\bullet}} 2NO + 2H_2O \xrightarrow{OH^{\bullet}} 2HNO_2 + 2H_2O \xrightarrow{OH^{\bullet}} 2NO_2 + 4H_2O \xrightarrow{OH^{\bullet}} 2HNO_3 + 4H_2O$$

At present, we do not know the exact pathway involved in the oxidation, and it is possible that the reaction might take place through some unidentified steps.[3] A detailed density functional theory (DFT) investigation is required to illustrate the mechanistic pathway for the transformation of N_2 to NO_3^- in the microbubbles.

https://doi.org/10.1021/jacs.4c11899
J. Am. Chem. Soc. XXXX, XXX, XXX–XXX

CONCLUSIONS

Our method provides a simple, one-step preparation of HNO_3 from air/N_2 under ambient conditions. No requirement for expensive chemicals, complicated procedures, or instrumentation suggests that the method is an affordable alternative to existing ones. Our microbubble method produces NO_3^- at a rate of 12.9 ± 0.05 μM h^{-1} without the use of an external electric potential or radiation. Moreover, this production rate remained relatively constant for many hours. The $OH^•$ generated from the Fenton's reaction at the droplet interface drives the oxidation of N_2 to NO_3^-. Fe^{2+} is regenerated by the in situ-produced H_2O_2 and plays the role of a catalyst in the transformation of N_2 to NO_3^-. We acknowledge that the limited production of H_2O_2 after a certain amount of time restricts the continuous production of NO_3^- at the current stage. A thorough understanding of the mechanistic pathways, enhanced production of H_2O_2 by modification of the experimental setup, and variation of parameters such as pH, catalyst, etc., is essential to create a more reactive interface that will enhance the NO_3^- yield.

ASSOCIATED CONTENT

Supporting Information

The Supporting Information is available free of charge at https://pubs.acs.org/doi/10.1021/jacs.4c11899.

Determination of H_2O_2; determination of NO_3^-; spin-trap measurements; quantification using mass spectrometry; and XPS spectra (PDF)

AUTHOR INFORMATION

Corresponding Author

Richard N. Zare − *Department of Chemistry, Stanford University, Stanford, California 94305, United States;* orcid.org/0000-0001-5266-4253; Email: zare@stanford.edu

Authors

Sandeep Bose − *Department of Chemistry, Stanford University, Stanford, California 94305, United States;* orcid.org/0000-0002-3471-5392

Mohammad Mofidfar − *Department of Chemistry, Stanford University, Stanford, California 94305, United States;* orcid.org/0000-0002-7160-8967

Complete contact information is available at: https://pubs.acs.org/10.1021/jacs.4c11899

Notes

The authors declare no competing financial interest.

ACKNOWLEDGMENTS

S.B. would like to thank the Nehru-Fulbright program for the fellowship. The authors thank the Air Force Office of Scientific Research through the Multidisciplinary University Research Initiative (MURI) program (AFOSR FA9550-21-1-0170) for supporting this project.

REFERENCES

(1) Nitric Acid Market Analysis: Industry Market Size, Plant Capacity, Production, Operating Efficiency, Demand & Supply, Type, End-User Industries, Sales Channel, Regional Demand, Foreign Trade, Company Share, Manufacturing Process, Policy and Regulatory Landscape, 2015-2032, 2024. https://www.chemanalyst.com/industry-report/nitric-acid-market-615.

(2) US EPA. AP 42 Chapter 8.8 Nitric Acid Production, 2024. https://gaftp.epa.gov/ap42/ch08/s08/final/c08s08_feb1998.pdf.

(3) Kumar, A.; Avadhani, V. S.; Nandy, A.; Mondal, S.; Pathak, B.; Pavuluri, V. K. N.; Avulapati, M. M.; Banerjee, S. Water Microdroplets in Air: A Hitherto Unnoticed Natural Source of Nitrogen Oxides. *Anal. Chem.* **2024**, *96*, 10515−10523.

(4) Lee, J. K.; Walker, K. L.; Han, H. S.; Kang, J.; Prinz, F. B.; Waymouth, R. M.; Nam, H. G.; Zare, R. N. Spontaneous Generation of Hydrogen Peroxide from Aqueous Microdroplets. *Proc. Natl. Acad. Sci. U.S.A.* **2019**, *116* (39), 19294−19298.

(5) Mehrgardi, M. A.; Mofidfar, M.; Zare, R. N. Sprayed Water Microdroplets Are Able to Generate Hydrogen Peroxide Spontaneously. *J. Am. Chem. Soc.* **2022**, *144*, 7606−7609.

(6) Kathmann, S. M.; Kuo, I.-F. W.; Mundy, C. J. Electronic Effects on the Surface Potential at the Vapor-Liquid Interface of Water. *J. Am. Chem. Soc.* **2008**, *130* (49), 16556−16561.

(7) Xiong, H.; Lee, J. K.; Zare, R. N.; Min, W. W. Strong Electric Field Observed at the Interface of Aqueous Microdroplets. *J. Phys. Chem. Lett.* **2020**, *11*, 7423−7428.

(8) Wei, H.; Vejerano, E. P.; Leng, W.; Huang, Q.; Willner, M. R.; Marr, L. C.; Vikesland, P. J. Aerosol Microdroplets Exhibit a Stable PH Gradient. *Proc. Natl. Acad. Sci. U.S.A.* **2018**, *115* (28), 7272−7277.

(9) Colussi, A. J. Mechanism of Hydrogen Peroxide Formation on Sprayed Water Microdroplets. *J. Am. Chem. Soc.* **2023**, *145*, 16315−16317.

(10) Song, X.; Meng, Y.; Zare, R. N. Spraying Water Microdroplets Containing 1,2,3-Triazole Converts Carbon Dioxide into Formic Acid. *J. Am. Chem. Soc.* **2022**, *144* (37), 16744−16748.

(11) Jin, S.; Chen, H.; Yuan, X.; Xing, D.; Wang, R.; Zhao, L.; Zhang, D.; Gong, C.; Zhu, C.; Gao, X.; Chen, Y.; Zhang, X. The Spontaneous Electron-Mediated Redox Processes on Sprayed Water Microdroplets. *JACS Au* **2023**, *3* (6), 1563−1571.

(12) Spoorthi, B. K.; Debnath, K.; Basuri, P.; Nagar, A.; Waghmare, U. V.; Pradeep, T. Spontaneous Weathering of Natural Minerals in Charged Water Microdroplets Forms Nanomaterials. *Science* **2024**, *384* (6699), 1012−1017.

(13) Zhu, C.; Pham, L. N.; Yuan, X.; Ouyang, H.; Coote, M. L.; Zhang, X. High Electric Fields on Water Microdroplets Catalyze Spontaneous and Fast Reactions in Halogen-Bond Complexes. *J. Am. Chem. Soc.* **2023**, *145* (39), 21207−21212.

(14) Vogel, Y. B.; Evans, C. W.; Belotti, M.; Xu, L.; Russell, I. C.; Yu, L.-J.; Fung, A. K. K.; Hill, N. S.; Darwish, N.; Gonçales, V. R.; Coote, M. L.; Swaminathan Iyer, K.; Ciampi, S. The Corona of a Surface Bubble Promotes Electrochemical Reactions. *Nat. Commun.* **2020**, *11* (1), No. 6323.

(15) Meng, Y.; Gnanamani, E.; Zare, R. N. One-Step Formation of Pharmaceuticals Having a Phenylacetic Acid Core Using Water Microdroplets. *J. Am. Chem. Soc.* **2023**, *145* (14), 7724−7728.

(16) Lee, J. K.; Samanta, D.; Nam, H. G.; Zare, R. N. Spontaneous Formation of Gold Nanostructures in Aqueous Microdroplets. *Nat. Commun.* **2018**, *9* (1), No. 1562.

(17) Banerjee, S.; Gnanamani, E.; Yan, X.; Zare, R. N. Can All Bulk-Phase Reactions Be Accelerated in Microdroplets? *Analyst* **2017**, *142* (9), 1399−1402.

(18) Yan, X.; Bain, R. M.; Cooks, R. G. Organic Reactions in Microdroplets: Reaction Acceleration Revealed by Mass Spectrometry. *Angew. Chem., Int. Ed.* **2016**, *55* (42), 12960−12972.

(19) Ghosh, J.; Cooks, R. G. Mass Spectrometry in Materials Synthesis. *TrAC, Trends Anal. Chem.* **2023**, *161*, No. 117010.

(20) Nandy, A.; Kumar, A.; Mondal, S.; Koner, D.; Banerjee, S. Spontaneous Generation of Aryl Carbocations from Phenols in Aqueous Microdroplets: Aromatic SN1 Reactions at the Air−Water Interface. *J. Am. Chem. Soc.* **2023**, *145* (29), 15674−15679.

(21) Bose, S.; Chatterjee, A.; Jenifer, S. K.; Mondal, B.; Srikrishnarka, P.; Ghosh, D.; Chowdhuri, A. R.; Kannan, M. P.; Elchuri, S. V.; Pradeep, T. Molecular Materials through Micro-

droplets: Synthesis of Protein-Protected Luminescent Clusters of Noble Metals. *ACS Sustainable Chem. Eng.* **2021**, *9* (12), 4554−4563.
(22) Satyabola, D.; Ahuja, T.; Bose, S.; Mondal, B.; Srikrishnarka, P.; Kannan, M. P.; Spoorthi, B. K.; Pradeep, T. Transformation of Nanodiamonds to Onion-like Carbons by Ambient Electrospray Deposition. *J. Phys. Chem. C* **2021**, *125* (20), 10998−11006.
(23) Ray Chowdhuri, A.; Spoorthi, B. K.; Mondal, B.; Bose, P.; Bose, S.; Pradeep, T. Ambient Microdroplet Annealing of Nanoparticles. *Chem. Sci.* **2021**, *12* (18), 6370−6377.
(24) Cassone, G.; Saija, F.; Sponer, J.; Shaik, S. The Reactivity-Enhancing Role of Water Clusters in Ammonia Aqueous Solutions. *J. Phys. Chem. Lett.* **2023**, *14*, 7808−7813.
(25) Zhang, D.; Wang, J.; Chen, H.; Gong, C.; Xing, D.; Liu, Z.; Gladich, I.; Francisco, J. S.; Zhang, X. Fast Hydroxyl Radical Generation at the Air-Water Interface of Aerosols Mediated by Water-Soluble $PM_{2.5}$ under Ultraviolet A Radiation. *J. Am. Chem. Soc.* **2023**, *145*, 6462−6470.
(26) Krushinski, L. E.; Vannoy, K. J.; Dick, J. E. Single Liquid Aerosol Microparticle Electrochemistry on a Suspended Ionic Liquid Film. *Small* **2024**, *20*, No. 2308637.
(27) Krushinski, L. E.; Qiu, L.; Dick, J. E. Levitating Droplet Electroanalysis. *Anal. Chem.* **2024**, *96*, 2764−2766.
(28) Rana, A.; Nguyen, J. H.; Renault, C.; Dick, J. E. Concentration Enrichment in a Dissolving Microdroplet: Accessing Sub-nanomolar Electroanalysis. *Anal. Chem.* **2024**, *96*, 5384−5391.
(29) Umar, M.; Aziz, H. A.; Yusoff, M. S. Trends in the Use of Fenton, Electro-Fenton and Photo-Fenton for the Treatment of Landfill Leachate. *Waste Manage.* **2010**, *30* (11), 2113−2121.
(30) Ganiyu, S. O.; Zhou, M.; Martínez-Huitle, C. A. Heterogeneous Electro-Fenton and Photoelectro-Fenton Processes: A Critical Review of Fundamental Principles and Application for Water/Wastewater Treatment. *Appl. Catal., B* **2018**, *235*, 103−129.
(31) Haber, F.; Weiss, J.; Pope, W. J. The Catalytic Decomposition of Hydrogen Peroxide by Iron Salts. *Proc. R. Soc. London, Ser. A* **1997**, *147* (861), 332−351.
(32) Fenton, H. J. H. LXXIII.—Oxidation of Tartaric Acid in Presence of Iron. *J. Chem. Soc. Trans.* **1894**, *65*, 899−910.
(33) Chen, S.; Liang, S.; Huang, R.; Zhang, M.; Song, Y.; Zhang, Y.; Tao, S.; Yu, L.; Deng, D. Direct Electroconversion of Air to Nitric Acid under Mild Conditions. *Nat. Synth.* **2024**, *3* (1), 76−84.
(34) Xing, D.; Meng, Y.; Yuan, X.; Jin, S.; Song, X.; Zare, R. N.; Zhang, X. Capture of Hydroxyl Radicals by Hydronium Cations in Water Microdroplets. *Angew. Chem., Int. Ed.* **2022**, *61* (33), No. e202207587.
(35) Li, J.; Xia, Y.; Song, X.; Chen, B.; Zare, R. N. Continuous Ammonia Synthesis from Water and Nitrogen via Contact Electrification. *Proc. Natl. Acad. Sci. U.S.A.* **2024**, *121* (4), No. e2318408121.
(36) Giwa, A. R. A.; Bello, I. A.; Olabintan, A. B.; Bello, O. S.; Saleh, T. A. Kinetic and Thermodynamic Studies of Fenton Oxidative Decolorization of Methylene Blue. *Heliyon* **2020**, *6* (8), 4−10.
(37) Mir, S. A. A Rapid Technique for Determination of Nitrate and Nitric Acid by Acid Reduction and Diazotization at Elevated Temperature. *Anal. Chim. Acta* **2008**, *620*, 183−189.
(38) Křepelová, A.; Newberg, J.; Huthwelker, T.; Bluhm, H.; Ammann, M. The Nature of Nitrate at the Ice Surface Studied by XPS and NEXAFS. *Phys. Chem. Chem. Phys.* **2010**, *12*, 8870−8880.
(39) Yamashita, T.; Hayes, P. Analysis of XPS Spectra of Fe^{2+} and Fe^{3+} Ions in Oxide Materials. *Appl. Surf. Sci.* **2008**, *254* (8), 2441−2449.
(40) Song, X.; Basheer, C.; Zare, R. N. Water Microdroplets-Initiated Methane Oxidation. *J. Am. Chem. Soc.* **2023**, *145* (50), 27198−27204.

https://doi.org/10.1021/jacs.4c11899
J. Am. Chem. Soc. XXXX, XXX, XXX−XXX